Supporting Information

Investigating Phosphorylation-induced Conformational Changes in WNK1 Kinase by Molecular Dynamics Simulations

Nisha Amarnath Jonniya, Md Fulbabu Sk, Parimal Kar *

Discipline of Biosciences and Biomedical Engineering, Indian Institute of Technology Indore, Khandwa Road, Indore-453552, MP, India

*Corresponding author. E-Mail: parimal@iiti.ac.in Phone: +91 732-430-6550

Contents

Table S1. Average SASA of Ser378, Ser382, and Thr386 for the complexes from the simulations in $Å^2$. Standard deviations are given in the parenthesis.

Systems	Avg. SASA ($Å^2$)	Avg. SASA ($Å^2$)	Avg. SASA ($Å^2$)
uWNK	$nSer^{378}$ = 56.7 (16.9)	$nSer^{382}$ = 44.5 (22.2)	Thr^{386} = 62.2 (25.7)
pWNK	$nSer^{378}$ = 53.8 (31.3)	$pSer^{382}$ = 153.6 (21.6)	Thr^{386} = 113.3 (18.0)
2pWNK	$pSer^{378}$ = 114.5 (20.1)	$pSer^{382}$ = 141.2 (16.8)	Thr^{386} = 106.0 (29.3)
u-Apo	$nSer^{378}$ = 53.5 (16.6)	$nSer^{382}$ = 42.5 (8.0)	Thr^{386} = 83.8 (19.1)
p-Apo	$nSer^{378}$ = 84.9 (14.4)	$pSer^{382}$ = 144.5 (18.9)	Thr^{386} = 119.9 (16.2)

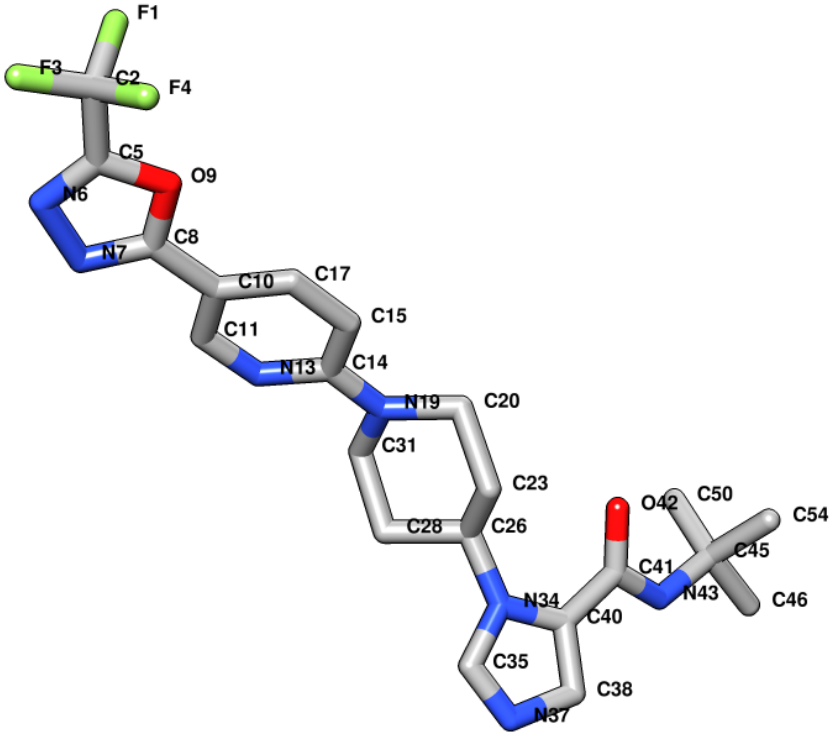

Figure S1. Chemical structure of WNK463 (ligand) in stick representation with labeled elements. Colors distinguish between carbon (grey), oxygen (red), nitrogen (blue), and fluroine (green).

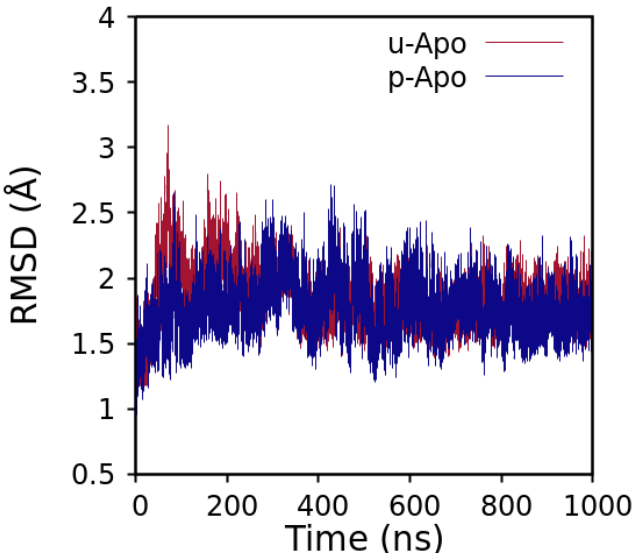

Figure S2. Time evolution of the root-mean-square deviations (RMSDs) of C_α atoms with respect to the initial structure for u-Apo (red) and p-Apo (blue) over 1μs simulations.

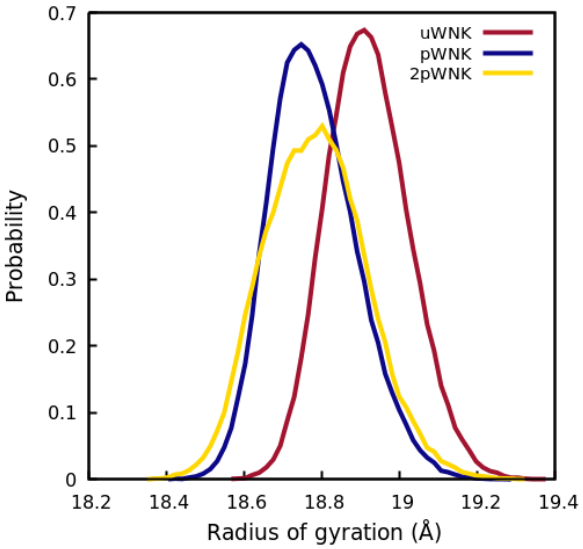

Figure S3. Probability distributions of the radius of gyration (R_g) of WNK complexes observed from the simulations of uWNK (red), pWNK (blue) and 2pWNK (gold).

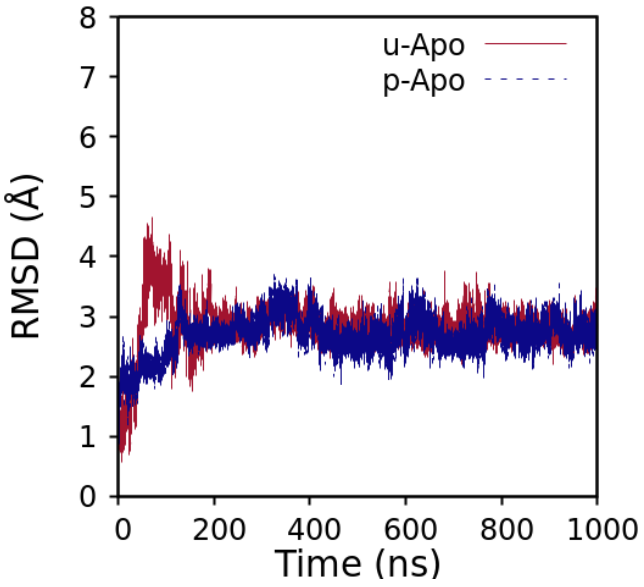

Figure S4. Time evolution of the root-mean-square deviations of C_α (RMSDs) of A-loop with respect to the initial structure for u-Apo (red) and p-Apo (blue) over 1μs simulations.

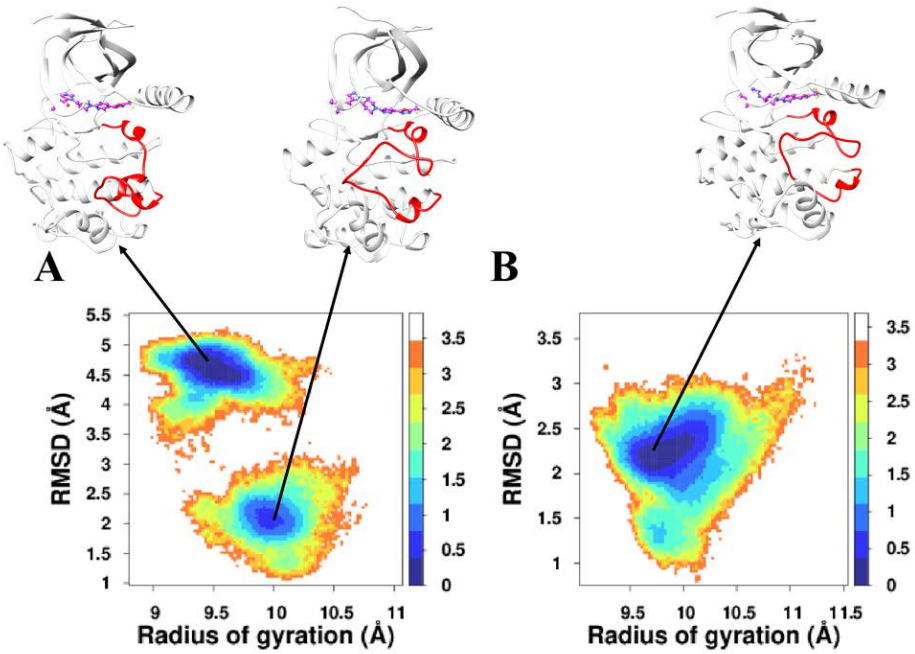

Figure S5. Two-dimensional free energy profile as a function of C_α RMSD of activation loop and its radius of gyration (R_g) from the MD simulations of (A) uWNK and (B) pWNK. Respective minimum free energy conformations are also represented.

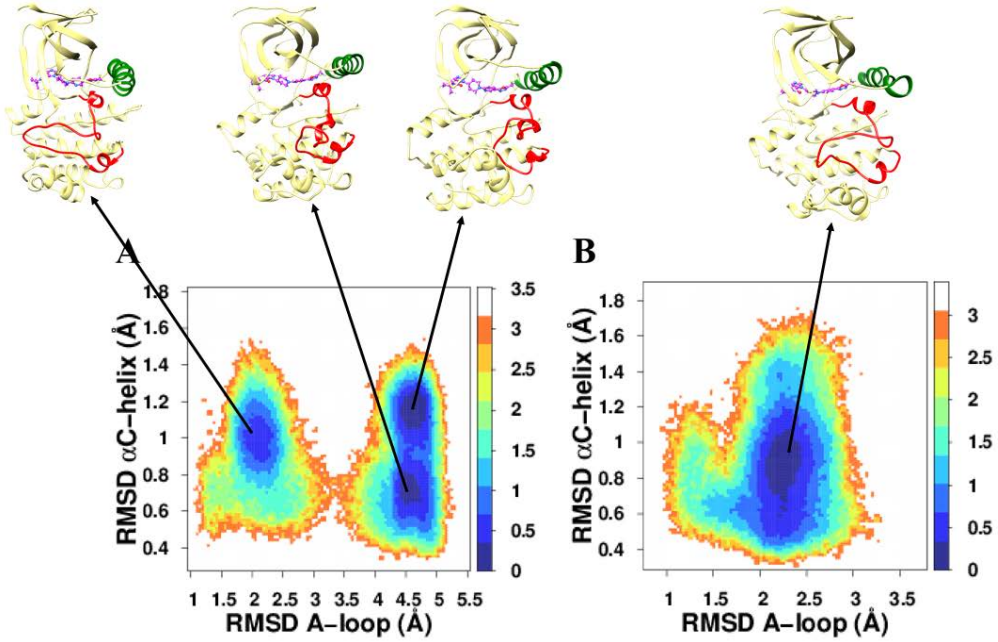

Figure S6: 2D free energy landscape as a function of RMSD of A-loop and RMSD of αC-helix during the MD simulations for (A) uWNK, and (B) pWNK, respectively. Respective minimum free energy conformations are also represented.

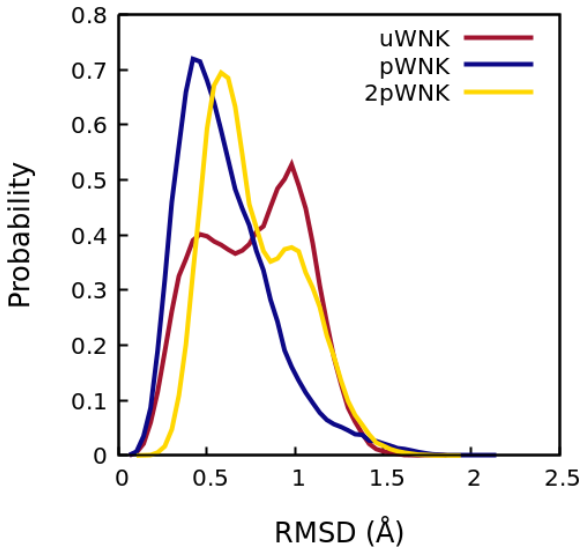

Figure S7. Probability distributions of the RMSD of C_α atoms of R-spine with respect to the initial structure of the uWNK (red), pWNK (blue) and 2pWNK (gold) complexes during simulations.

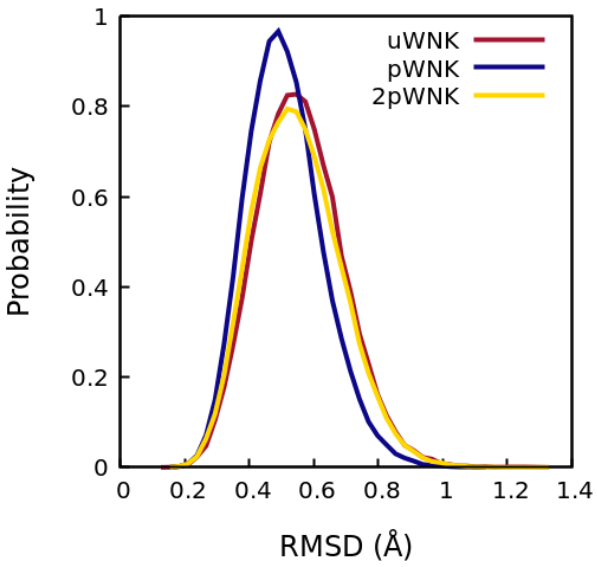

Figure S8. Probability distributions of the RMSD of C_α atoms of C-spine with respect to the initial structure of the uWNK (red), pWNK (blue) and 2pWNK (gold) complexes during simulations.

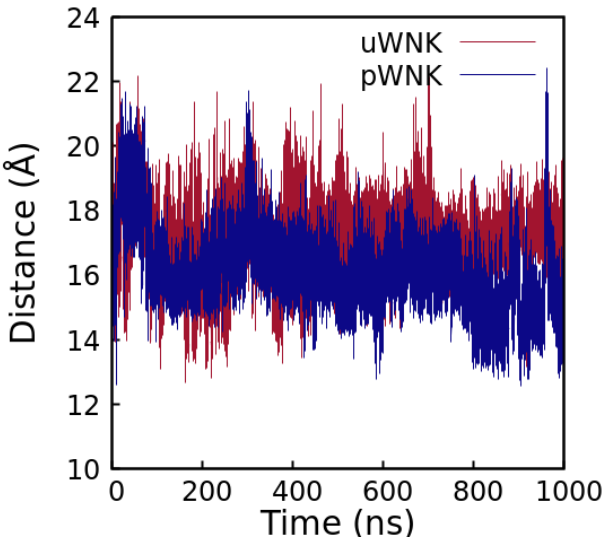

Figure S9. The distance between the NZ of Lys(K233) and CD of Glu(E268) calculated from the simulations of uWNK (red) and pWNK (blue).

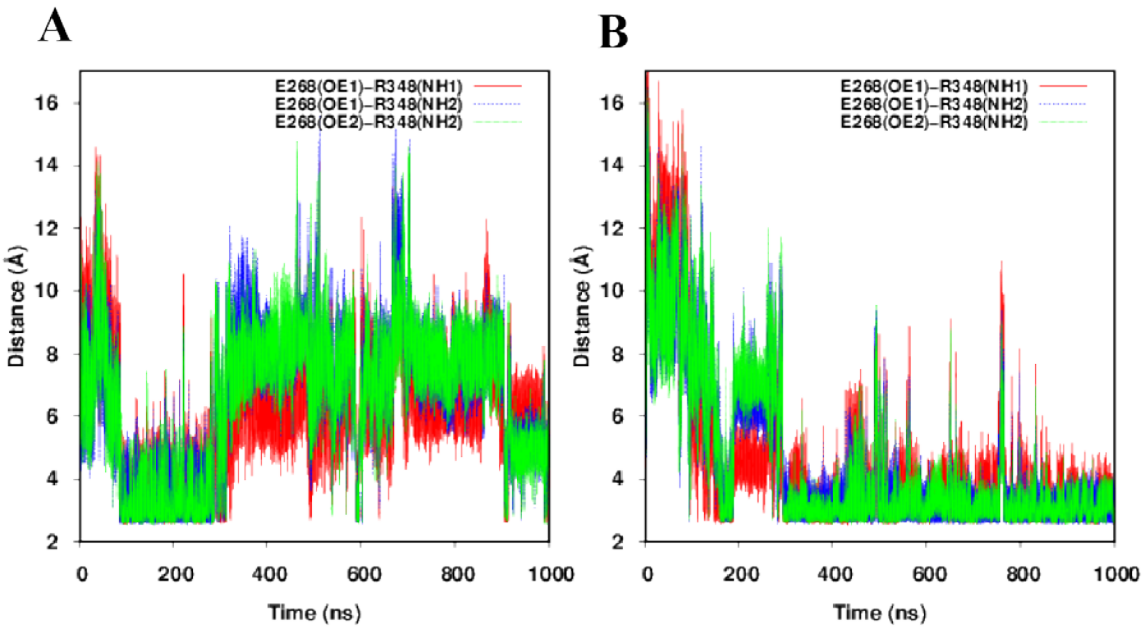

Figure S10. Various interactions between residues of E268 and R348 with different atoms from the simulations for (A) uWNK (B) pWNK.

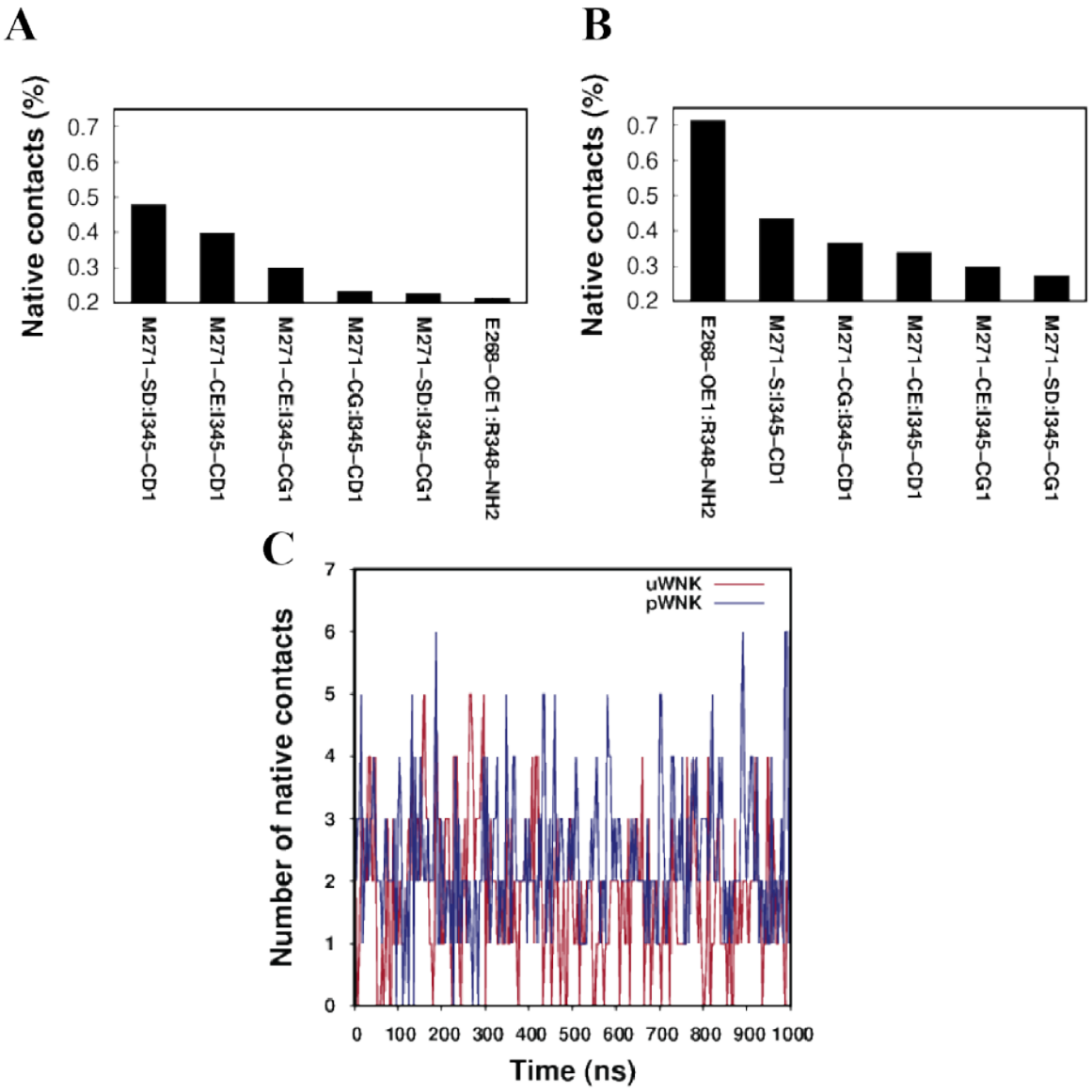

Figure S11: Percentage native contacts between αC-helix and catalytic loop from the MD simulations are shown for (A) uWNK and (B) pWNK, respectively. (C) The number of native contacts throughout the MD simulations for uWNK (red) and pWNK (blue), respectively.

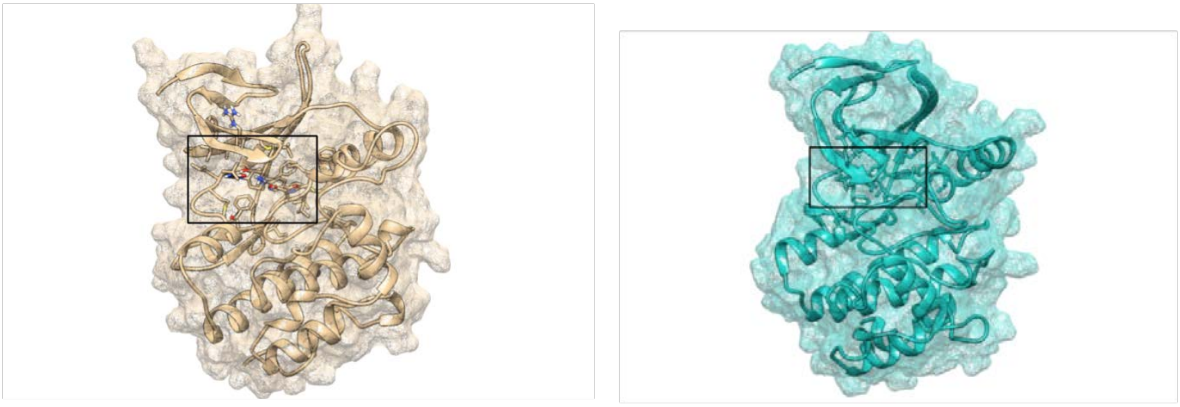

Figure S12. Structural differences in the ATP binding pocket of unphosphorylated (uWNK-grey) (left) and phosphorylated (pWNK-sea green) (right) with ATP/inhibitor pocket (black rectangle).

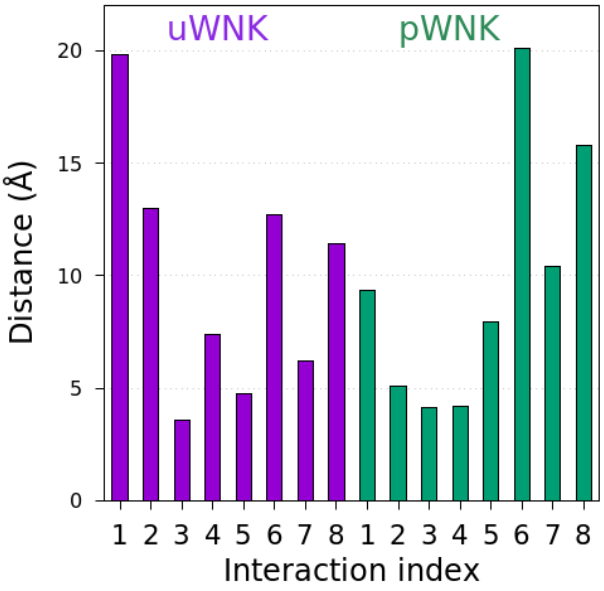

Figure S13. Interactions controlling stability and dynamics of A-loop and αC-helix with indices: (1) for S382 OH-K256 NZ, (2) S382 OH-R255 CZ, (3) D349 CG-K375 NZ, (4) R348 NH1-E268 OE1, (5) E268 OE2-R264 NH1, (6) S382 OH-R348 CZ, (7) S382 OH-R376 CZ, and (8) S382 OH-D349 CG, respectively. Bars represent the average distance determined from the MD simulations. Phosphorylated complex in purple and unphosphorylated complex in green are shown.

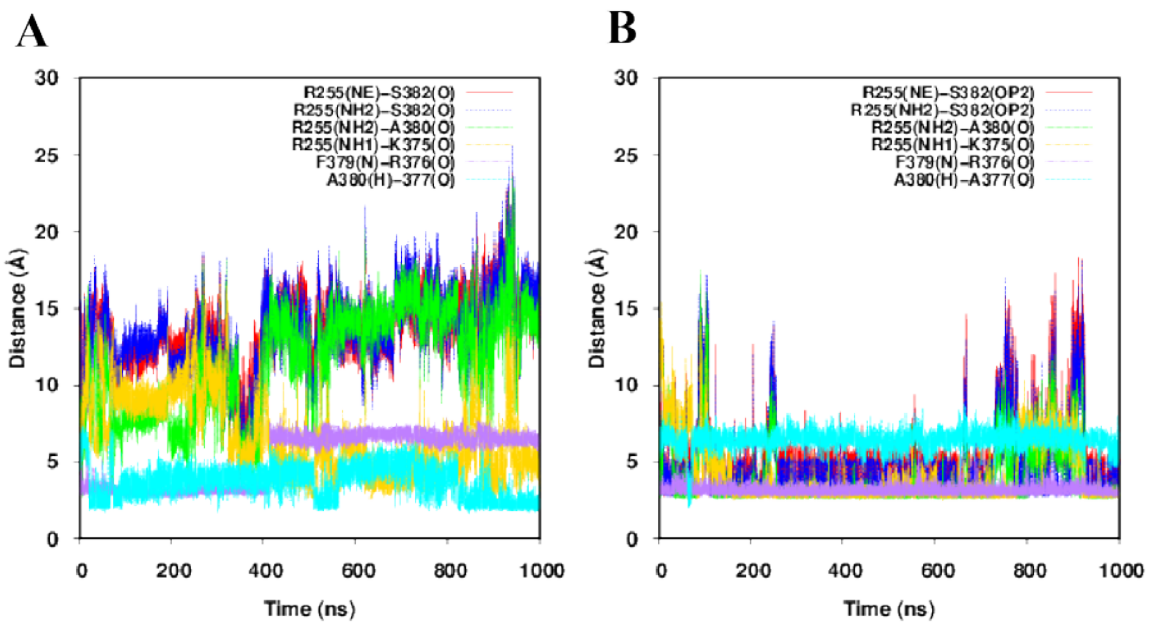

Figure S14. Various interactions between residues S382-R255 with different atoms and other interactions involved in A-loop from the simulations for (A) uWNK (B) pWNK

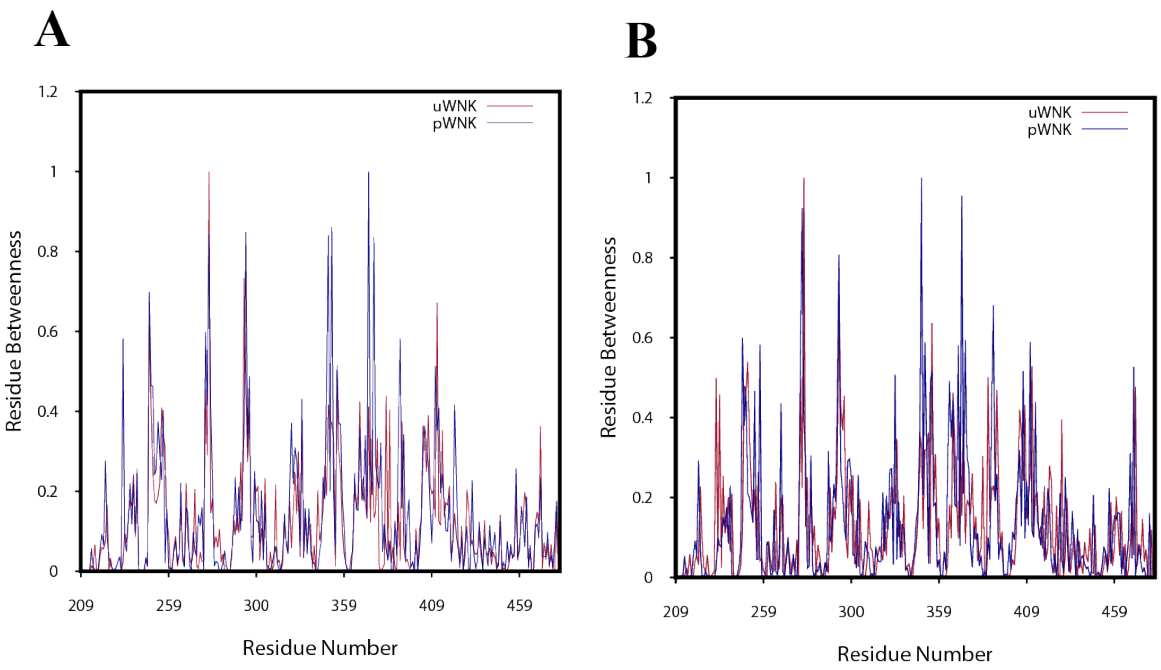

Figure S15. Residue betweenness as a function of residues calculated via NAPS for uWNK and pWNK complexes (A) as well as Apo systems (B), respectively.

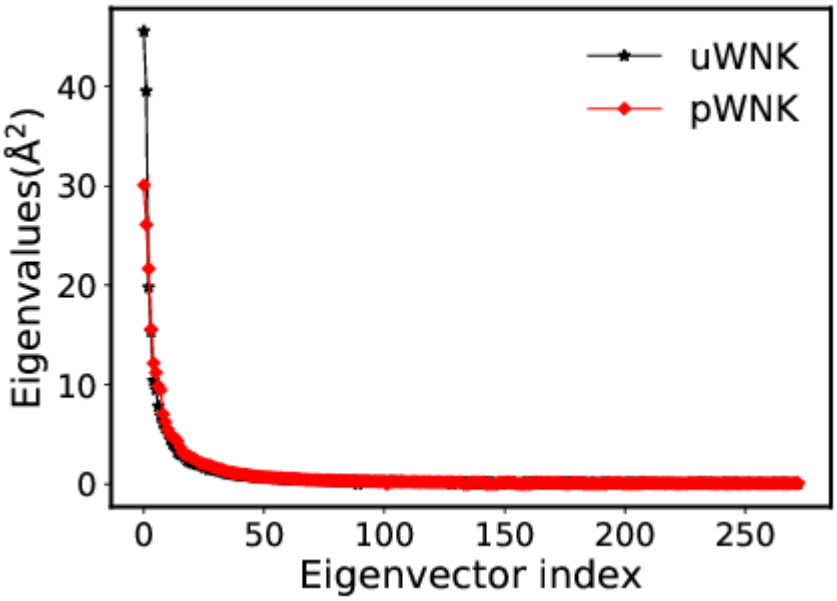

Figure S16. Comparison of the eigenvalues plotted against the corresponding eigenvector indices from the C_α covariance matrix constructed from the simulations of uWNK and pWNK systems.

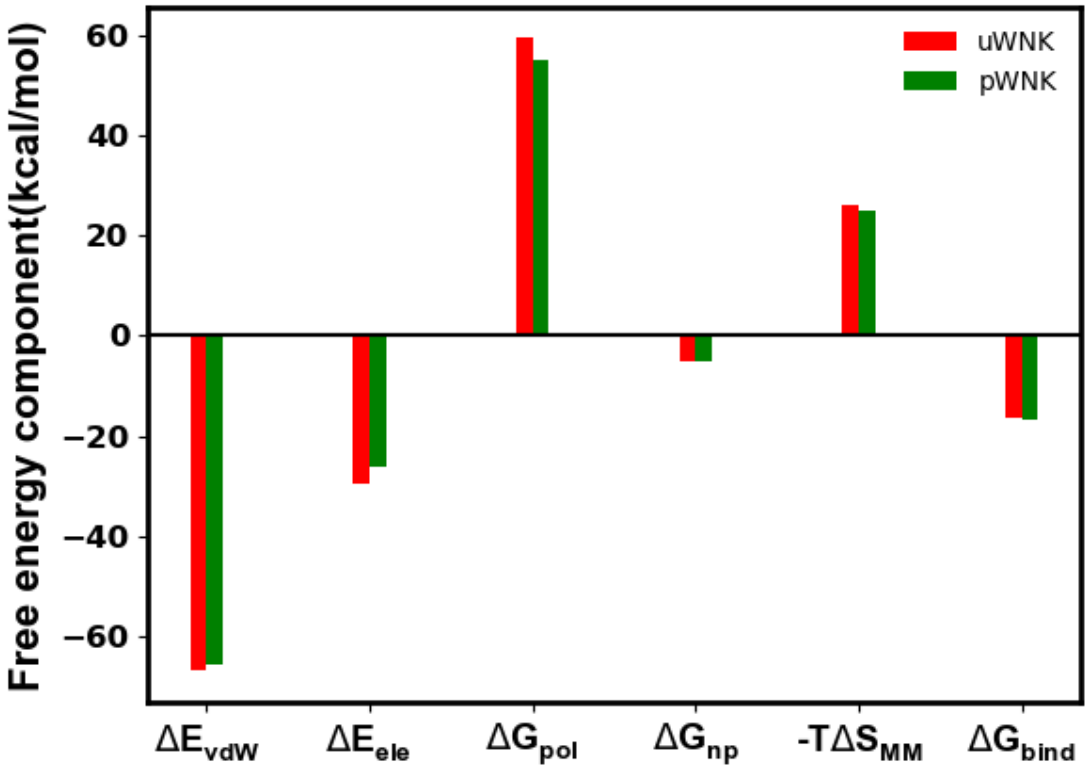

Figure S17. Energy components (kcal/mol) for the binding of WNK463 (ligand) to the WNK1 kinase domain. ΔE_{vdW}, van der Waals energy; ΔE_{ele}, electrostatic energy in the gas phase; ΔG_{pol}, polar solvation energy; ΔG_{np}, non-polar solvation energy; $T\Delta S$, entropy contribution; ΔG_{bind} = ΔH-TΔ S

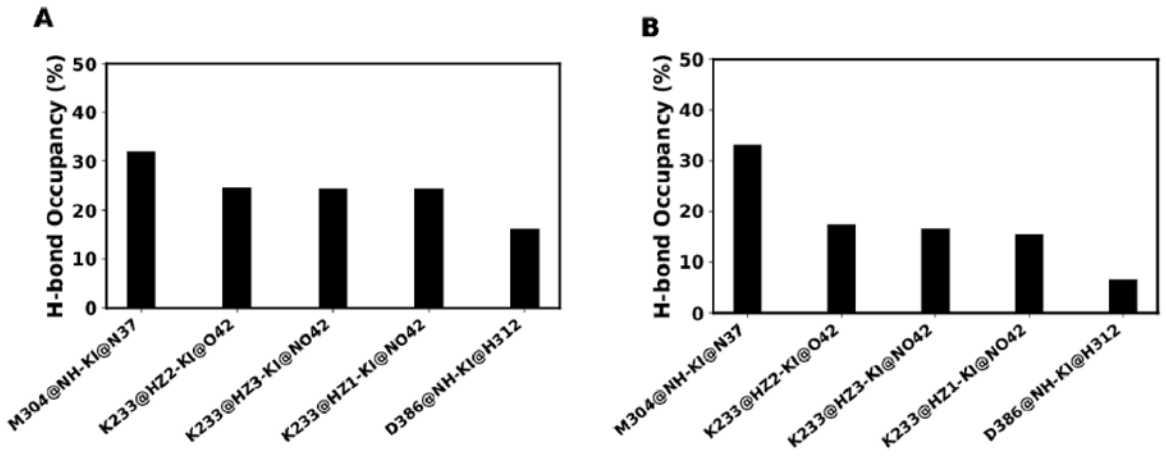

Figure S18. Hydrogen bond interactions between particular residues of protein and kinase inhibitor over the last 600 ns of simulations for (A) uWNK and (B) pWNK, respectively.

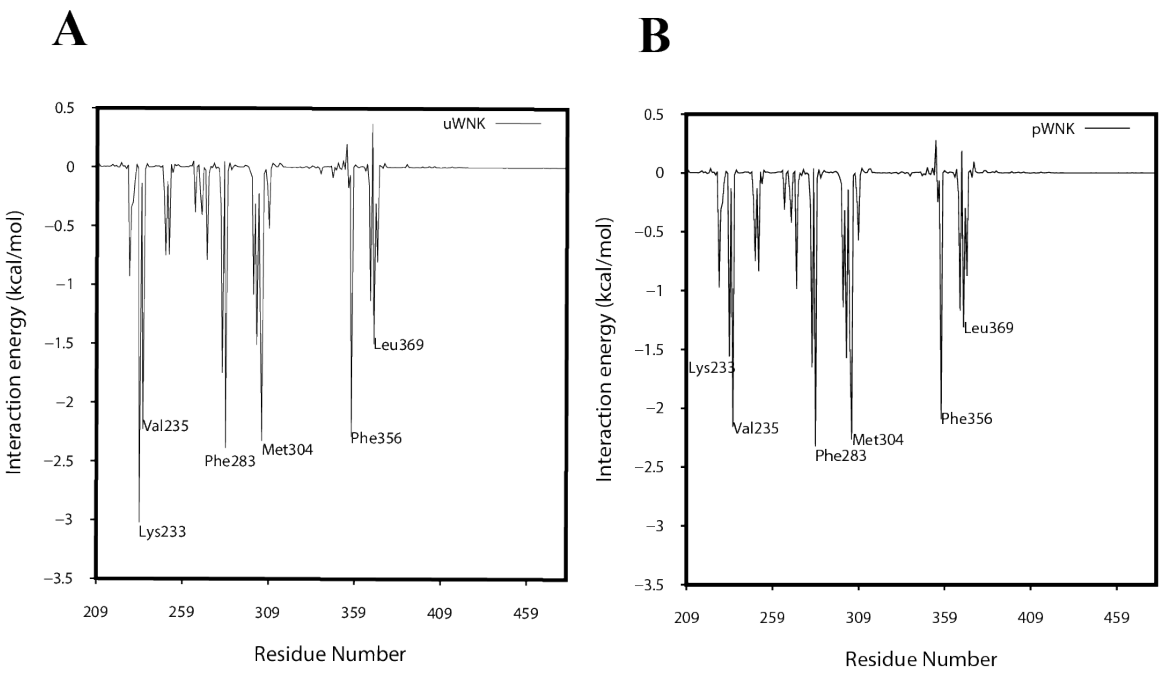

Figure S19. Decomposition of the binding free energy into contributions from individual residues for uWNK (A) and pWNK (B), respectively.

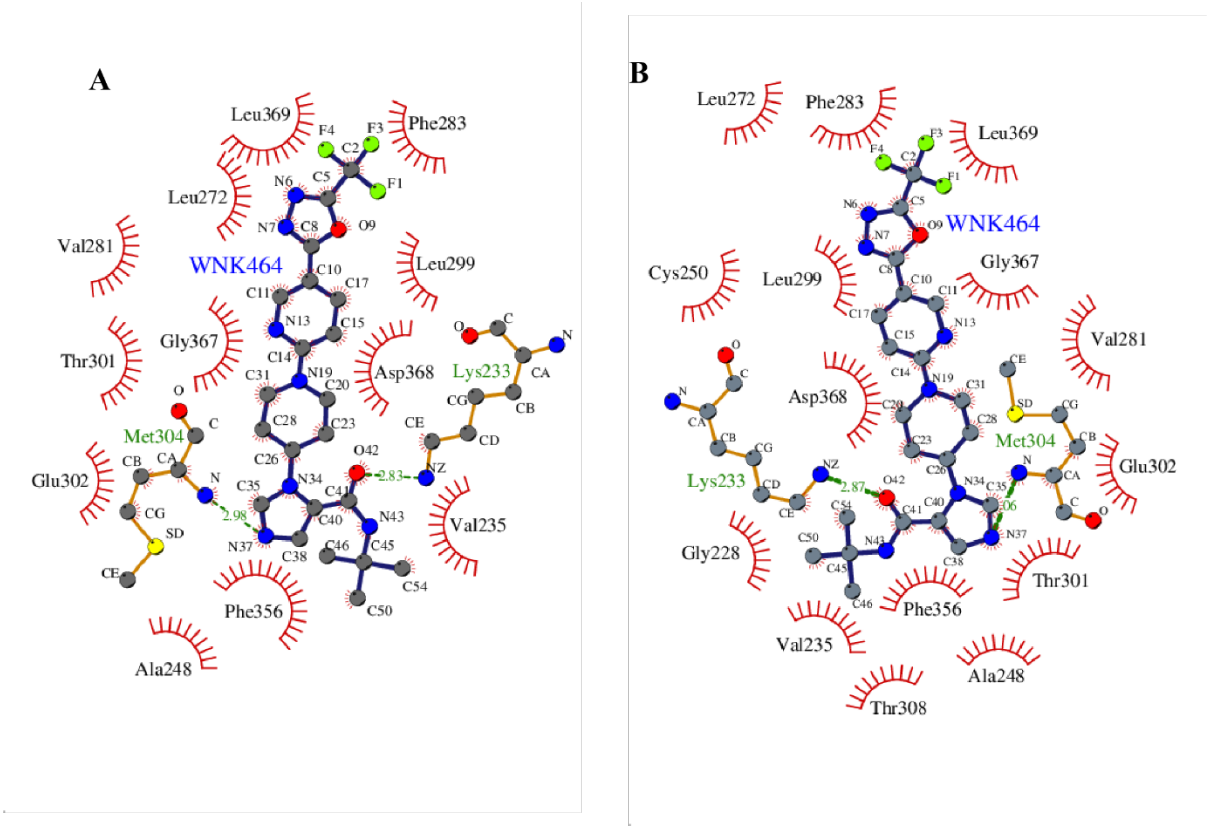

Figure S20. Ligand-Protein interaction diagrams for (A) uWNK and (B) pWNK. The plots were generated by Ligplot+. Hydrogen bonds are shown as green dotted lines, while hydrophobic contacts are represented by an arc with spokes radiating towards the ligand atoms they contact.

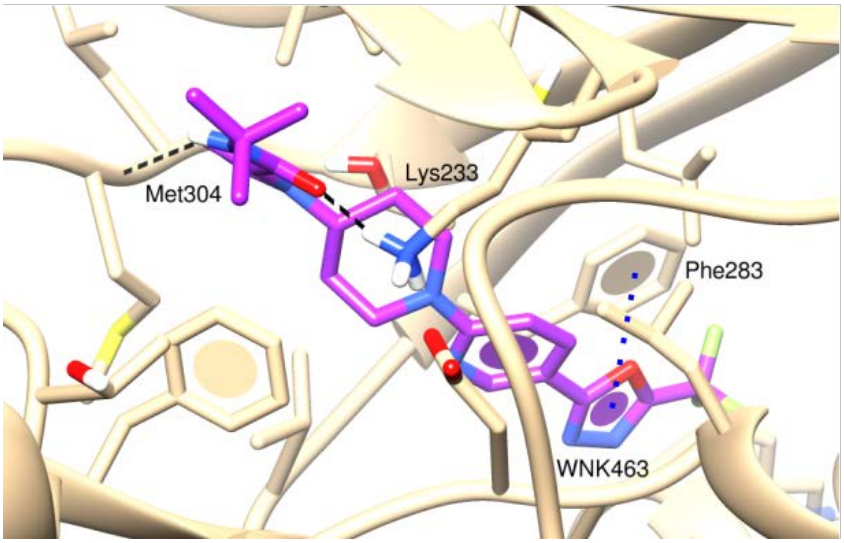

Figure S21. H-bond and π-π interaction between WNK1 kinase and ligand (WNK463). 3D plot for the H-bond and π–π interaction for the uWNK complex. Similar interactions were observed for pWNK.

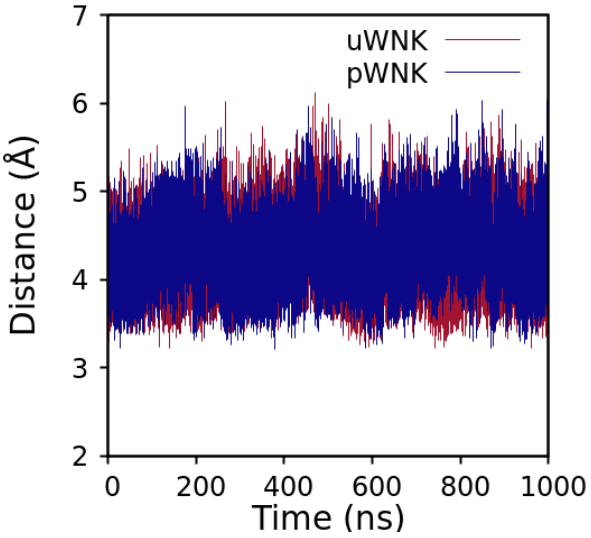

Figure S22. π-π interaction distance calculated between CD of Phe283 phenyl ring and oxadiazole of ligand (WNK463) throughout the MD simulations for uWNK (red) and pWNK (blue) during simulations.